UC San Diego

UC San Diego Previously Published Works

Title

Intrinsically Stretchable Block Copolymer Based on PEDOT:PSS for Improved Performance in Bioelectronic Applications

Permalink

https://escholarship.org/uc/item/17v802qz

Journal

ACS Applied Materials and Interfaces, 14(4)

ISSN

1944-8252

Authors

Blau, Rachel
Chen, Alexander X.
Polat, Beril
et al.

Publication Date

2022-02-02

Data Availability

Associated data will be made available after this publication is published.

Peer reviewed

eScholarship.org Powered by the California Digital Library
University of California

ACS APPLIED MATERIALS & INTERFACES

www.acsami.org

Research Article

Intrinsically Stretchable Block Copolymer Based on PEDOT:PSS for Improved Performance in Bioelectronic Applications

Rachel Blau, Alexander X. Chen, Beril Polat, Laura L. Becerra, Rory Runser, Beeta Zamanimeymian, Kartik Choudhary, and Darren J. Lipomi*

Cite This: *ACS Appl. Mater. Interfaces* 2022, 14, 4823−4835

Read Online

ACCESS | Metrics & More | Article Recommendations | Supporting Information

Downloaded via UNIV OF CALIFORNIA SAN DIEGO on July 29, 2023 at 13:14:18 (UTC).
See https://pubs.acs.org/sharingguidelines for options on how to legitimately share published articles.

ABSTRACT: The conductive polyelectrolyte complex poly(3,4-ethylenedioxythiophene):poly(styrenesulfonate) (PEDOT:PSS) is ubiquitous in research dealing with organic electronic devices (e.g., solar cells, wearable and implantable sensors, and electrochemical transistors). In many bioelectronic applications, the applicability of commercially available formulations of PEDOT:PSS (e.g., Clevios) is limited by its poor mechanical properties. Additives can be used to increase the compliance but pose a risk of leaching, which can result in device failure and increased toxicity (in biological settings). Thus, to increase the mechanical compliance of PEDOT:PSS without additives, we synthesized a library of intrinsically stretchable block copolymers. In particular, controlled radical polymerization using a reversible addition−fragmentation transfer process was used to generate block copolymers consisting of a block of PSS (of fixed length) appended to varying blocks of poly(poly(ethylene glycol) methyl ether acrylate) (PPEGMEA). These block copolymers ($PSS_{(1)}$-*b*-$PPEGMEA_{(x)}$, where *x* ranges from 1 to 6) were used as scaffolds for oxidative polymerization of PEDOT. By increasing the lengths of the PPEGMEA segments on the PEDOT:[$PSS_{(1)}$-*b*-$PPEGMEA_{(1−6)}$] block copolymers, ("Block-1" to "Block-6"), or by blending these copolymers with PEDOT:PSS, the mechanical and electronic properties of the polymer can be tuned. Our results indicate that the polymer with the longest block of PPEGMEA, Block-6, had the highest fracture strain (75%) and lowest elastic modulus (9.7 MPa), though at the expense of conductivity (0.01 S cm^{-1}). However, blending Block-6 with PEDOT:PSS to compensate for the insulating nature of the PPEGMEA resulted in increased conductivity [2.14 S cm^{-1} for Blend-6 (2:1)]. Finally, we showed that Block-6 outperforms a commercial formulation of PEDOT:PSS as a dry electrode for surface electromyography due to its favorable mechanical properties and better adhesion to skin.

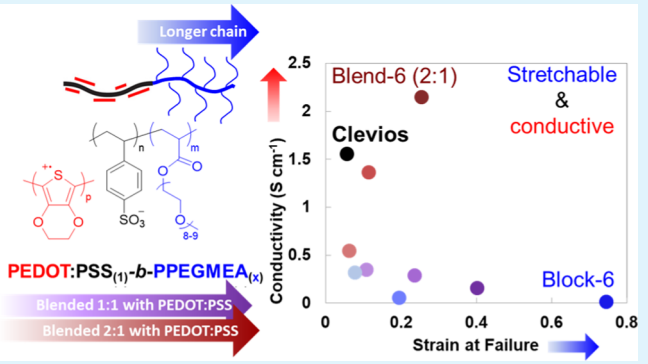

KEYWORDS: *PEDOT:PSS, organic electronics, stretchable electronics, electromyography (EMG), RAFT polymerization, block copolymers*

1. INTRODUCTION

The polyelectrolyte complex poly(3,4-ethylenedioxythiophene):poly(styrenesulfonate) (PEDOT:PSS) is ubiquitous in organic electronics and bioelectronics.[1] Its transmissivity makes it attractive for photovoltaic applications (e.g., solar cells)[2−5] and light-emitting devices,[6,7] and it is among the best organic thermoelectric materials.[8,9] Moreover, PEDOT:PSS exhibits mixed modes of conductivity—electronic and ionic[10,11]—which facilitates interactions with biological structures,[12] gaining great interest in organic electrochemical transistors for biosensors.[1,13−15] PEDOT:PSS consists of short chains of PEDOT complexed with longer chains of PSS by coulombic interactions. When cast into a solid film, PEDOT:PSS exhibits conductivity values of 0.1−10 S cm^{-1},[16] which is dependent on the ratio of PEDOT to PSS[17] and solid content of the dispersion.[18] Several approaches for enhancing the conductivity and stretchability of PEDOT:PSS have been studied in recent years,[17] reaching conductivity values[18−22] as high as 4380 S cm^{-1} and fracture strains up to 800%.[23] Likewise, the electronic characteristics of PEDOT:PSS can be manipulated by thermal processes (e.g., annealing),[24] exposure to light,[25] blending with an ionic liquid (IL),[23,26] or the addition of a strong acid.[27−29]

The electronic properties of PEDOT:PSS are highly dependent on the morphology of the solid film, which is in part determined by the solubility, kinetics of solidification, and thermal history, all of which depend on the molecular

Received: September 28, 2021
Accepted: January 11, 2022
Published: January 24, 2022

© 2022 American Chemical Society

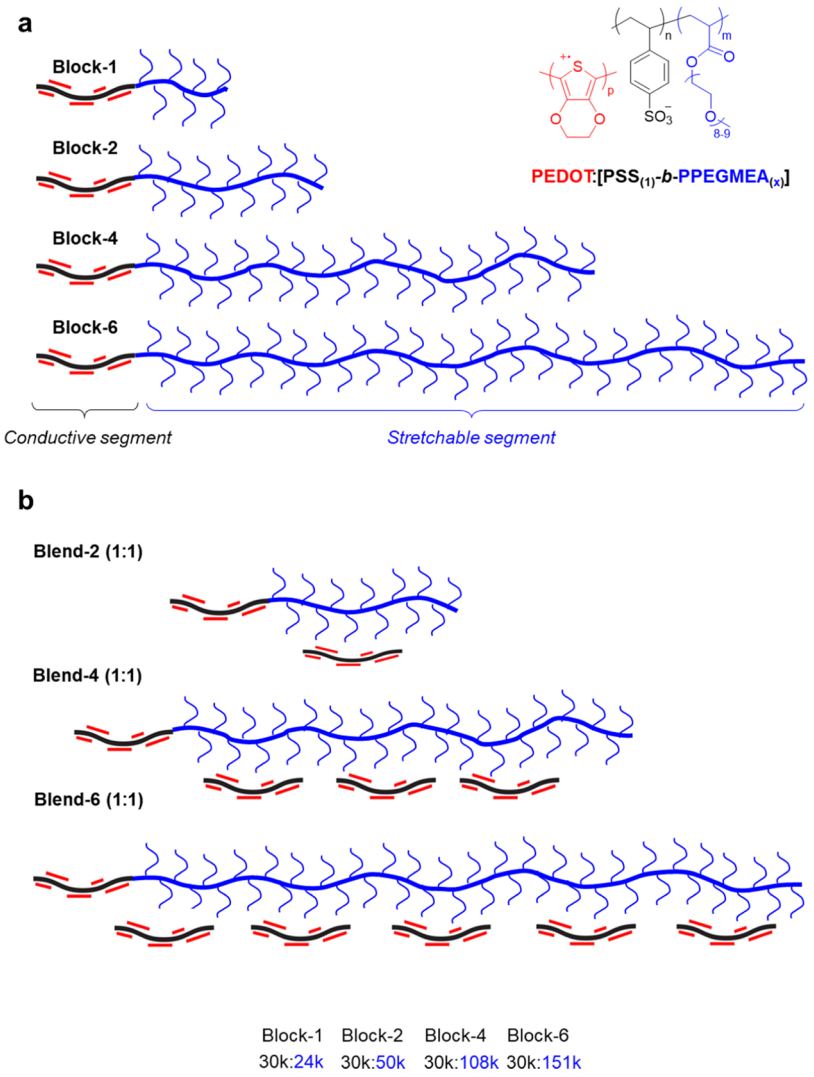

Figure 1. Schematic representation of the block copolymers and their physical blends. (a) PEDOT:[$PSS_{(1)}$-*b*-$PPEGMEA_{(x)}$] block copolymers were synthesized to have increasing lengths of PPEGMEA (blue) attached to PSS (black). Conductive segments of PEDOT (red) are coulombically associated with the PSS. (b) PEDOT:PSS was blended with PEDOT:[$PSS_{(1)}$-*b*-$PPEGMEA_{(x)}$] in ratios of 1:1 or 2:1 wt % (Scheme S1). Molecular weights (M_n) of PSS and PPEGMEA chains were calculated according to the ^{1}H NMR of the crude polymer.

structure. Previous works by Timpanaro et al.[30] and Crispin et al.[31] suggest that solid PEDOT:PSS morphology consists of closely packed PEDOT-rich domains in a PSS-rich matrix. Adding a co-solvent additive, typically a high-boiling, polar molecule [e.g., DMSO,[32] ethylene glycol,[33] or polyethylene glycol (PEG)[34] has been shown to increase the conductivity by several orders of magnitude. Although the mechanism by which polar additives improve the electrical conductivity of PEDOT:PSS films is not well understood, several studies have provided evidence of secondary doping effects[35] (e.g., phase separation of excess PSS resulting in reduced insulation and formations of larger PEDOT domains). Mengistie et al. showed that adding ethylene glycol (up to 6 wt %) or PEG (up to 2 wt %) to solutions of PEDOT:PSS led to increased conductivity dependent on the molecular weight or chain length of the additive.[34] Palumbiny et al. showed that the addition of ethylene glycol in a PEDOT:PSS film results in stronger interchain coupling of both PEDOT and PSS molecules (e.g., smaller $\pi-\pi$ stacking distances), as well as increased crystallinity and edge-on texturing in PEDOT domains, thus improving film morphology for charge transport.[36] Likewise, Rivnay et al. demonstrated that doping with EG results in changes in the microstructure of the PEDOT:PSS film (e.g., an increase in particle size and film heterogeneity), which contributes to improved charge conduction pathways.[10] Crispin et al. showed that the addition of diethylene glycol led to changes in the morphology of the film and a concomitant improvement in three-dimensional (3D) charge conduction.[31]

Recent applications of PEDOT:PSS—e.g., flexible optoelectronic and bioelectronic devices—have demanded substantially greater degrees of mechanical compliance than are possible with commercial formulations. Current commercial PEDOT:PSS formulations often yield films that have an elastic modulus on the order of ∼100 MPa and <10% fracture strain. However, bioelectronic devices that can be interfaced with the skin or implanted in the body require an elastic modulus closer to that of the tissue it interfaces with (e.g., 5 kPa-140 MPa for skin[37] and <1 kPa for brain tissue).[38−40] Likewise, these devices must be able to withstand far greater strains based on their application (e.g., ∼30% for skin[41] and ∼100% for joints[42]) in order to minimize interfacial stress and match the

https://doi.org/10.1021/acsami.1c18495
ACS Appl. Mater. Interfaces 2022, 14, 4823−4835

Scheme 1. Synthesis of PEDOT:[$PSS_{(1)}$-*b*-$PPEGMEA_{(x)}$] *block* Copolymer Library[a]

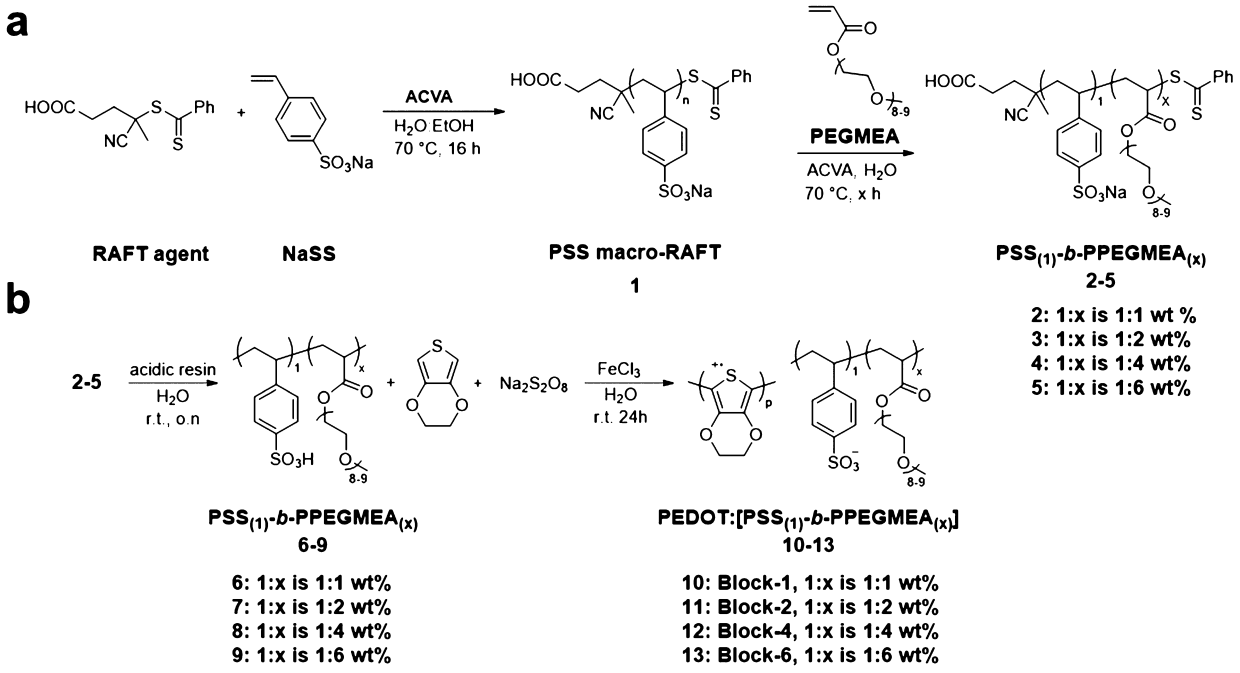

[a](a) Two-step RAFT polymerization of block copolymers $PSS_{(1)}$-*b*-$PPEGMEA_{(x)}$ (2−5). RAFT polymerization of the PSS macro-RAFT precursor 1 and subsequent preparation of PEDOT:[$PSS_{(1)}$-*b*-$PPEGMEA_{(x)}$], 2−5. (b) Oxidative polymerization of PEDOT on the block copolymer library scaffolds.

curvature of the organ. The most common approach to solving this problem has been to increase the stretchability[43] of PEDOT:PSS by blending it with plasticizers such as ILs,[23,26] xylitol,[44] Zonyl,[45] and D-sorbitol.[46,47] In addition to small molecule additives, a more recent approach for increasing the conductivity and modulating the mechanical properties of PEDOT:PSS for bioelectronic applications is the incorporation of biocompatible ILs.[48] However, many low molecular weight additives pose the risk of leaching out of the polymer matrix (e.g., due to phase separation over time, pH, temperature, and exposure to liquids). The consequences of potential leaching effects can result in (1) a reduction of the mechanical compliance of PEDOT:PSS, (2) potential damage to or failure of the electronic device, and (3) in biological settings, a risk of toxicity for nonbiocompatible plasticizers. Polymeric additives as blends are less susceptible to leaching compared to small molecules and provide an alternative route to tuning the mechanical properties of PEDOT:PSS. Li et al. demonstrated that blending PEDOT:PSS with PEG results in a decreased elastic modulus and increased fracture strain relative to a pure PEDOT:PSS film, while still resulting in an increase in conductivity.[49] Chen et al. showed that the electrical properties of PEDOT:PSS were improved by mixing with polyvinyl alcohol.[50] Further details on the mechanical properties of PEDOT:PSS blends with small molecule and polymer additives have been discussed elsewhere.[51,52] However, few studies have explored the effect of these polar species covalently bound to PEDOT:PSS. Recently, our group published the design and synthesis of an intrinsically stretchable PEDOT:PSS-based elastomer.[53,54] Briefly, PEDOT was synthesized on a scaffold where the polyanion PSS was covalently linked to poly(poly(ethylene glycol) methyl ether acrylate) (PPEGMEA), rendering it stretchable. This block copolymer (PEDOT:[$PSS_{(1)}$-*b*-$PPEGMEA_{(x)}$]) showed a lower modulus and higher failure strain relative to PEDOT:PSS but also showed a lower conductivity. Therefore, the purpose of this study is to explore synthetic derivatives of this copolymer in order to improve the mechanical properties (e.g., modulus, fracture strain, and toughness) for bioelectronic applications. As an example, we demonstrate the fabrication of electromyogram (EMG) recording electrodes without the use of small-molecule additives and cosolvents.

To accomplish this goal, we synthesized a library of polymers characterized by increasing length of the stretchable, bottlebrush-like PPEGMEA segments, while keeping a constant length of the PSS segment. The ratios of PSS to PPEGMEA were 1:1, 1:2, 1:4, and 1:6. These scaffolds were rendered conductive by oxidative polymerization of PEDOT, and a constant ratio of PEDOT to PSS was used for all four components of this library (Figure 1a). These polyelectrolyte materials, with the general form PEDOT:[$PSS_{(1)}$-*b*-PPEG-$MEA_{(x)}$], were named Block-1, Block-2, Block-4, and Block-6, where x = 1, 2, 4, and 6. We reasoned that increasing the length of the soft, insulating PPEGMEA chain would enable greater energy dissipation and result in a lower elastic modulus, greater toughness, and greater fracture strain, but at the expense of the conductivity.

To compensate for the decrease of conductivity relative to increasing PPEGMEA chain length, we blended the copolymers with PEDOT:PSS (synthesized in-house). We reasoned that the PEDOT:PSS segments would fill void spaces and increase the ratio of conductive versus insulating components. In addition, we hypothesized that (in comparison to other reported polymer blends) forming a polymeric blend with PEDOT:PSS would result in less phase segregation due to the similarity in chemical composition, dispersity, and molecular weight. These blends have a 1:1 wt % ratio of total PEDOT:PSS (i.e., both covalently bound to the block

https://doi.org/10.1021/acsami.1c18495
ACS Appl. Mater. Interfaces 2022, 14, 4823−4835

copolymer and the added PEDOT:PSS) to PPEGMEA (Figure 1b). We refer to these blends as Blend-2 (1:1), Blend-4 (1:1), and Blend-6 (1:1). In some experiments, we explored the effects of greater concentrations of PEDOT:PSS (2:1 wt %) in these blended matrices (e.g., Blend-1 (2:1), Blend-2 (2:1), Blend-4 (2:1), and Blend-6 (2:1)).

2. EXPERIMENTAL SECTION

2.1. General. Number-average molecular weight (M_n), weight-average molecular weight (M_w), and dispersity ($Đ$) were determined using an Agilent Technologies 1260 Infinity II LC system. The mobile phase was 30% methanol and 70% 0.2 M $NaNO_3$ and 0.01 M NaH_2PO_4 in water at pH 7 (adjusted with concentrated NaOH) at 40 °C at 1 mL min^{-1}. The column used was PL aquagel-OH Mixed-B column, calibrated against narrow dispersity PSS standards (purchased from Polymer Standards Service). ^{1}H NMR spectra were acquired in D_2O at room temperature on a Bruker AVANCE III 600 MHz NMR spectrometer fitted with a 1.7 mm triple resonance probe with the z-gradient.

2.2. Materials. Sodium 4-styrenesulfonate (NaSS), 4,4′-azobis(4-cyanovaleric acid) (ACVA), azobis(isobutyronitrile) (AIBN), PEGMEA (M_n = 480 g mol^{-1}), 4-cyano-4-(phenylcarbonothioylthio)-pentanoic acid (the reversible addition fragmentation transfer (RAFT) chain transfer agent), and ethylenedioxythiophene (EDOT) were purchased from Sigma-Aldrich and used without further purification. Distilled water filtered using a Milli-Q purification system was used throughout.

2.3. Synthesis of the Library Components Using RAFT Polymerization. *2.3.1. PSS Macro-RAFT Precursor 1 Synthesis.* Traditionally, the synthesis of PSS is a two-step process involving the anionic polymerization of polystyrene (PS) followed by sulfonation. This process can result in incomplete sulfonation and synthetic defects (e.g., formation of sulfones and cross-links in the polymer chain).[55] In contrast, RAFT synthesis is tolerant to aqueous solutions, thus enabling a controlled polymerization of the water-soluble monomer sodium styrene sulfonate (NaSS) to create a fully sulfonated PSS with a predictable molecular weight.[56] Thus, we used RAFT polymerization for both the synthesis of the PSS precursor (i.e., PSS macro-RAFT **1**) as well as the $PSS_{(1)}$-*b*-$PPEGMEA_{(x)}$ (**2-5**) library. Poly(styrene sulfonate sodium salt) (PSSNa, PSS macro-RAFT 1) was synthesized as previously described.[54] Briefly, NaSS (12.24 g, 59.4 mmol), the RAFT agent 4-cyano-4-(phenylcarbonothioylthio)pentanoic acid (110.4 mg, 0.4 mmol), and ACVA (22.4 mg, 0.08 mmol) were dissolved in 42 mL of water and 17 mL of ethanol and degassed by purging with nitrogen for 30 min. The reaction mixture was placed in an oil bath at 70 °C and left to react for 16 h (Scheme 1a). The reaction was stopped by exposure to air. PSS macro-RAFT **1** was purified by precipitation in acetone and dried under vacuum to afford a pink powder (11.7 g, 95% yield; GPC: M_n = 23.8 kDa, M_w = 31.2 kDa, $Đ$ = 1.3.

2.3.2. RAFT Polymerization of $PSS_{(1)}$-b-$PPEGMEA_{(X)}$ block Copolymer Library (2–5). PSS macro-RAFT 1 (2.094 g, 0.07 mmol), PEGMEA in different amounts according to desired length (6.72, 10.08, and 13.44 g, 14 mmol, for x = 1, 1.8, 4, and 6.3, respectively), and ACVA (3.93 mg, 0.014 mmol) were dissolved in 54 mL of water and degassed under a flow of nitrogen for 30 min. The reaction mixture was placed in an oil bath at 70 °C for 0.75, 1, 2.5, and 4 h for x = 1, 1.8, 4, and 6.3, respectively (Scheme 1a, Table 1). The reactions were stopped by rapid cooling on dry ice and exposure to air. The ^{1}H NMR of the crude mixtures showed 25, 69, 75, and 79% PEGMEA conversion, respectively (Table 1). (Note: allowing the reaction to proceed to higher conversion led to an increase in the dispersity.) The reaction mixture was lyophilized to circa 10 mL, before adding 10 mL of acetone. The slurry was washed 2× with 50 mL of diethyl ether. This process was repeated three times. The resulting solid was recovered by vacuum filtration using a 10 μm disposable filter and dried under vacuum to afford a sticky pink solid (PSS:PPEGMEA mass ratio was determined by ^{1}H NMR: 1:1, 1:1.8, 1:4, 1:6.3, and molecular weights were determined by GPC: M_n = 32.6 kDa, M_w = 45.2 kDa, $Đ$ = 1.38, M_n = 35.3 kDa, M_w = 52.8 kDa, $Đ$ = 1.5, M_n = 29.7 kDa, M_w = 66.6 kDa, $Đ$ = 2.2, M_n = 47.2 kDa, M_w = 100 kDa, $Đ$ = 2.1, respectively).

Table 1. Summary of Ratio between Monomers (PSS:PEGMEA), Ratio between PSS Macro-RAFT Agent (RAFT) and Initiator (I), Monomer Conversions, and Reaction Times for Each Library Component

PSS-*b*-PPEGMEA ratio[a] (wt %)	[PEGMEA]:[RAFT[b]]:[I]	PPEGMEA monomer conv (%)[c]	reaction time (h)
1:1	200:1:0.2	25	0.75
1:2	150:1:0.2	69	1
1:4	300:1:0.2	75	3
1:6	400:1:0.2	79	4.5

[a]The wt % ratio of PSS to PPEGMEA was obtained by ^{1}H NMR of the purified polymer in D_2O. [b]PSS macro-RAFT polymer precursor. [c]Obtained by ^{1}H NMR of the crude polymer in D_2O.

2.3.3. Viscosity Measurements. $PSS_{(1)}$-*b*-$PPEGMEA_{(x)}$ block copolymers were dissolved in MiliQ water (10 mg mL^{-1}), and 100 μL aliquots were injected into a RheoSense microVISCTM viscometer in triplicates.

2.3.4. Synthesis of PEDOT:[$PSS_{(1)}$-b-$PPEGMEA_{(x)}$] Library (10–13). This synthesis was modified from our previous report.[54] A constant ratio of PEDOT:PSS (1:1.3 by weight) was kept for all library components, regardless of PPEGMEA chain length. The derivatives of PEDOT:[$PSS_{(1)}$-*b*-$PPEGMEA_{(x)}$] are referred to as Block-1, Block-2, Block-4, and Block-6 for x = 1, 1.8, 4, and 6.3, respectively. To generate the acidified polymer, 1.5 g of $PSS_{(1)}$-*b*-$PPEGMEA_{(x)}$ (**2–5**) was dissolved in MilliQ water (c = 40, 40, 50, and 75 mg mL^{-1} for x = 1, 1.8, 4, and 6.3, respectively) and stirred over acidic resin (Dowex Marathon C hydrogen form) for 18 h. The dissolved polymer solutions were filtered over a 10 μm filter, obtaining acidified compounds **6–9**. Sodium persulfate (1150 mg, 4.83 mmol) and iron trichloride (100 wt % in water, 0.175 mL) were added to the filtrates of 1300, 1778, 3250, and 4745 mg $PSS_{(1)}$-*b*-$PPEGMEA_{(x)}$ polymers (32.5, 22.2, 65, and 63 mL, respectively) (Scheme 1b). The portion of PSS (650 mg) in the block copolymer was kept constant for all components of the library. The solution was vigorously stirred before the addition of EDOT (500 mg, 3.51 mmol). After 1 h, an additional 37–67 mL of MilliQ water were added to prevent gelation of the mixture and maintain a final volume of 100 mL. The reaction was left to react for 24 h at room temperature. PEDOT:[$PSS_{(1)}$-*b*-$PPEGMEA_{(x)}$] (Block-1, Block-2, Block-4 and Block-6) was purified by stirring over acidic resin (Dowex Marathon C hydrogen form, 17 g) and basic resin (Lewatit MP-62 free base, 11 g) for 6 h, followed by a 10 μm filtration.

2.3.5. Synthesis of PEDOT:PSS. We synthesized PEDOT:PSS instead of using a commercially available formulation in order to (1) ensure that the PEDOT:PSS possessed a similar molecular weight to the PEDOT:PSS segment on the block copolymer, (2) avoid the presence of additives used in commercial formulations that improve stability and conductivity, and (3) ensure complete sulfonation of PSS using RAFT polymerization. The oxidative polymerization of EDOT was described in our previously reported synthesis.[54] Briefly, PSS was dissolved in water (50 mg mL^{-1}) and stirred over an acidic resin (Dowex Marathon C hydrogen form) for 18 h at room temperature. The acidified PSS was filtered through a 1 μm filter. The ratio of PEDOT:PSS was similar to that of commercially available formulation, Clevios PH 1000 (1:2.5 wt %). Sodium persulfate (1175 mg, 2.3 wt equiv) and iron trichloride (0.178 mL of 100 wt % solution) were then added to 23.5 mL of this solution (PSS: 1175 mg, 2.3 wt equiv), along with an additional 50 mL of water. The reaction was stirred for 10 min before the addition of EDOT (511 mg, 1 wt equiv). The reaction was stirred vigorously at room temperature for 24 h. PEDOT:PSS was purified over 17 g of acidic (Dowex Marathon C hydrogen form) and 11 g of basic (Lewatit MP-62 free base) resins for 6 h and then filtered through a 10 μm filter.

https://doi.org/10.1021/acsami.1c18495
ACS Appl. Mater. Interfaces 2022, 14, 4823–4835

Table 2. Summary of the Mole (mol %) and Mass (wt %) Ratios of PSS to PPEGMEA[a]

polymer	PSS:PPEGMEA ratio[b](mol %)	PSS:PPEGMEA ratio[b](wt %)	M_n theo[c] (g/mol)	M_w exp[d] (g/mol)	$Đ$[d]
PSS macro-RAFT	N.A.	N.A.	30,000	31,000	1.3
$PSS_{(1)}$-*b*-$PPEGMEA_{(1)}$	1:0.435	1:1	54,400	45,000	1.385
$PSS_{(1)}$-*b*-$PPEGMEA_{(2)}$	1:0.79	1:2	80,000	53,000	1.496
$PSS_{(1)}$-*b*-$PPEGMEA_{(4)}$	1:1.7	1:4	138,000	66,500	2.24
$PSS_{(1)}$-*b*-$PPEGMEA_{(6)}$	1:2.7	1:6	181,000	100,000	2.11

[a]Theoretical (theo) and experimental (exp) molecular weights were determined by ^{1}H NMR and GPC, respectively. ($Đ$, dispersity.) [b]PSS:PPEGMEA ratio was obtained by ^{1}H NMR of the purified polymer in D_2O. [c]Determined by ^{1}H NMR of the crude polymer (i.e., sample containing unreacted monomers) in D_2O. [d]Obtained by size exclusion chromatography in a 70/30 (v/v) ratio of aqueous phosphate buffer to methanol.

2.3.6. Blending Library Components. All library components were blended with PEDOT:PSS (synthesized as described above) to maintain a ratio of 1:1 wt % between PEDOT:PSS to PPEGMEA (0.6 wt % and higher). These blends are referred to as Blend-2 (1:1), Blend-4 (1:1), and Blend-6 (1:1). Similarly, blends with ratios of 2:1 wt% (PEDOT:PSS relative to PPEGMEA) were prepared as well [Blend-2 (2:1), Blend-4 (2:1), Blend-6 (2:1)].

2.4. Film Casting. Substrates of either silicon or glass (25 mm × 25 mm) were first activated with an oxygen plasma to increase hydrophilicity. Then, 0.3 mL of each block copolymer derivative was drop-cast on the substrate and left to dry in a desiccator containing Drierite for 48−72 h at room temperature until the formation of a solid film.

2.5. Preparation of Samples for Conductivity Measurements. Glass slides were cut into 25 mm squares with a diamond-tipped scribe. The slides were then cleaned by successively sonicating in Alconox solution (2 mg mL^{-1} in water), deionized water, acetone, and isopropyl alcohol for 10 min each and dried with compressed air. The glass slides were then plasma treated (~30 W, ~200 mTorr) for 3 min to remove any residual organic material and expose the hydroxyl groups on the substrate surface. The PEDOT block copolymer derivatives were spin-coated onto glass slides at a spin speed of 500 rpm (250 rpm s^{-1} ramp) for 120 s followed by 2000 rpm (1000 rpm s^{-1} ramp) for 30 s to form homogenous and semitransparent films (Figure S1). After spin-coating, the samples were annealed on a hotplate at 120 °C for 15 min in air. The resistances of the films were measured using a four-point probe wired to a Keithley 2400 sourcemeter. The thickness of the films was measured using a Dektak XT profilometer, and the cross-sectional area was used to convert resistance to conductivity. The conductivity, σ, was calculated from an average of three samples using the following equations

$$R_s = \frac{\pi}{\ln(2)} R \quad (1)$$

$$\sigma = \frac{1}{t \times R_s} \quad (2)$$

where R is the resistance measured by the four-point probe, R_s is the sheet resistance, and t is the thin film thickness. A correction factor of 0.7744 was applied according to the geometry of the measurement.[57]

2.6. Tensile Tests. Solutions of PEDOT derivatives (1 mL) were drop-cast into an inverse dogbone mold milled from a block of Teflon (l = 1.3 cm, w = 0.7 cm). The mold containing PEDOT solution was left to dry in a desiccator containing Drierite for 48−96 h at room temperature (with derivatives containing longer blocks of PPEGMEA taking longer to dry). Fully dried dogbones were carefully removed from the Teflon mold using tweezers. We were unable to successfully form dogbones of PEDOT:PSS and Block-1 due to cracking of the sample when drying. Thus, Clevios was used as a proxy. The edges of the dogbone samples (i.e., where excess solution dried to form a thick border around the sample) were then carefully trimmed using scissors. The ends of the dogbones were wrapped with electrical tape to ensure that fracture did not occur under the grips of a linear actuator. These dogbones were then placed in 3D-printed grips attached to a 10 N force gauge on a Mark-10 linear actuator and elongated at a strain rate of 1 mm min^{-1} until fracture. Force-elongation data were converted to stress−strain data using the dimensions of each dogbone (the thickness of each sample was measured after fracture using a Dektak XT profilometer). For some samples, the resistance was measured simultaneously. For these measurements, bare copper wires (one on each side of the dogbone) were adhered to the dogbone underneath the electrical tape using carbon paint. These copper wires were connected to alligator probes attached to a Keithley 2400 sourcemeter.

2.7. Characterization of Free-Standing Film Adhesion to Glass and Plastic Substrates. To conduct a 90° peel test, a Mark-10 linear actuator equipped with the peel test accessory kit was operated in the upright position. The plastic substrate (Petri dish) or glass substrate (glass microscope slide) was fixed to the sliding plate using double-sided tape. Rectangular polymer films (6 × 2 cm) were produced using a 3D-printed mold (6 × 2 cm) and procedures described in Section 2.9.1. The free-standing films were lightly pressed onto the substrate and attached to a grip connected to a 0.5 N force gauge. The films were delaminated at a rate of 330 mm min^{-1} to obtain a plot of force relative to displacement (travel). The steady-state adhesive force was calculated by averaging the longest plateau on the force-displacement plot.

2.8. Impedance Spectroscopy Measurements. Free standing films were sandwiched between two stainless steel electrodes (cross-sectional area = 5 mm × 5 mm). A Biologic SP-200 Potentiostat was used in conjunction with ECLab software version 11.32. The measurement frequencies were logarithmic, and 10 frequencies per decade were used. The measurements were performed from 3 MHz to 100 mHz with an amplitude of 10 mV AC and a zero DC offset. The data were fitted with a complex nonlinear least square fitting method with ECLab software version 11.32. The measurement frequencies are for the two-contact measurement, and the working electrode is connected to either of the contacts on the polymer films. The results are presented in the form of Nyquist plots, the real and imaginary impedances, and the impedance magnitude (Figure S11).

2.9. Application as EMG Electrodes. *2.9.1. EMG electrode fabrication.* A square mold (2 cm × 2 cm, 2 mm depth) was 3D-printed using polylactic acid (LulzBot TAZ 5 3D printer, Loveland, CO). A mold release spray (Ease Release 200, Mann Release Technologies) was used to coat the surface of the mold before drop-casting 0.8 mL of filtered (1 μm glass fiber filter) Block-6, Blend-6, and Clevios (as a control) in the mold. The molds containing PEDOT solution were dried at 60 °C on a hotplate for 2 h, and the dried films were gently removed from the mold after they cooled down to rt. To fabricate the electrode, a bare copper wire was attached to the back of the film using carbon paint and then covered with carbon tape to ensure good connectivity.

2.9.2. Forearm EMG Measurements. For the EMG measurements, the electrodes were pressed firmly onto the skin of the forearm to ensure good contact. For Clevios and Blend-6 electrodes, Tegaderm was used to tape the electrodes to skin. Block-6 electrodes were sufficiently adhesive without Tegaderm. The copper wires of the electrodes were connected to the ECG channel of a MAX30001-EVSYS evaluation board (Maxim Integrated Products, Inc.). The reference electrode (3 M Ag/AgCl Red Dot Monitoring Electrode) was placed on the elbow of the same arm and connected to the Body

https://doi.org/10.1021/acsami.1c18495
ACS Appl. Mater. Interfaces 2022, 14, 4823−4835

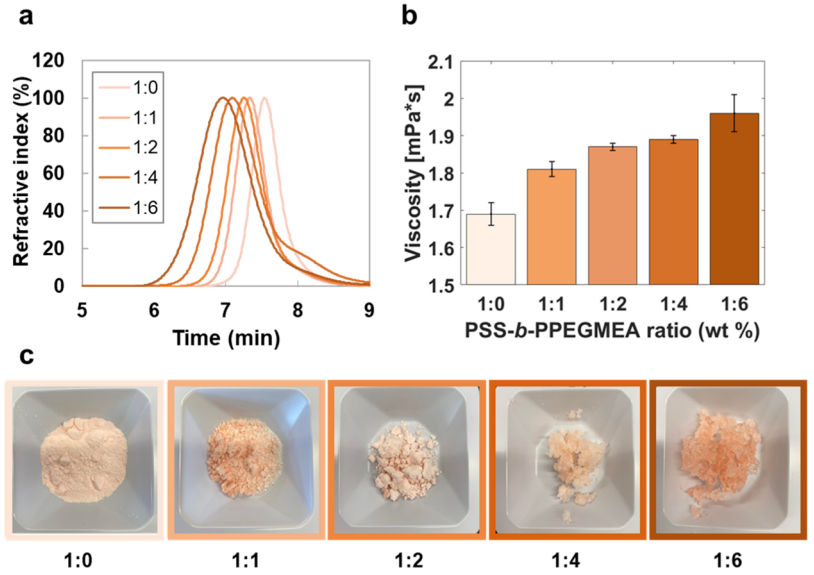

Figure 2. Physicochemical characterization of the $PSS_{(1)}$-*b*-$PPEGMEA_{(x)}$ library. (a) Stacked GPC traces of $PSS_{(1)}$-*b*-$PPEGMEA_{(x)}$ synthesized with different amounts of PEGMEA. The legend shows the mass (wt %) ratio of PSS to PPEGMEA in each trace (where 1:0 wt % corresponds to the PSS macro-RAFT precursor). (b) Viscosity measurements of the library components in solution (10 mg mL^{-1}). (c) Photographs showing that an increase in the PPEGMEA chain length from 1:0 (powder) to 1:6 (gel-like solid) results in a stickier solid.

Bias pin of the board. The ECG channel was configured to have a gain of 20 V/V and a sampling rate of 512 readings s^{-1}. Post-ADC digital filters were used during the recordings. The low pass filter cutoff was 40 Hz, and the high pass filter cutoff was 0.5 Hz. A Butterworth notch filter with a width of 59 to 61 Hz was applied post-measurement to eliminate 60 Hz power-line noise.[58] The signal-to-noise ratio (SNR) was calculated from the root mean square (RMS) of the filtered data and the ratio between four peaks and their base line. We performed on-body EMG measurements with two subjects. We used a protocol approved by the Internal Review Board at the University of California San Diego Human Research Protections Program (Project # 191950S).

3. RESULTS AND DISCUSSION

3.1. Characterization of PEDOT:[$PSS_{(1)}$-*b*-$PPEGMEA_{(x)}$]. The UV absorbance spectra were analyzed for the different block copolymers to confirm that the chemistry of PEDOT was not significantly influenced by the change in the block copolymer backbone. Figure S1a shows a negligible difference in the normalized absorbance spectra. The molecular weight, wt % ratios of PSS to PPEGMEA, and purity of the library of $PSS_{(1)}$-*b*-$PPEGMEA_{(x)}$ were characterized by gel permeation chromatography (GPC) and ^{1}H NMR (Table 2, Figures S2–S6). Higher ratios of PPEGMEA to PSS (and longer reaction times) resulted in higher molecular weights of the block copolymer (ranging from 31 kDa for the PSS macro-RAFT to 100 kDa for $PSS_{(1)}$-*b*-$PPEGMEA_{(6)}$), as determined by GPC (Figure 2a). Viscosity measurements showed that copolymer derivatives containing longer PPEGMEA chains were also more viscous (Figure 2b). An increase in the PPEGMEA chain length from 1:0 (powder) to 1:6 resulted in a stickier, gel-like solid (Figure 2c, Movie S1). Surface morphology was characterized by atomic force microscopy (AFM) (Figures S7 and S8) and scanning electron microscopy (SEM) (Figures S9 and S10).

3.2. Thin-Film Conductivity of PEDOT:[$PSS_{(1)}$-*b*-$PPEGMEA_{(x)}$]. We explored the effect of the increasing PPEGMEA block on the conductivities of the PEDOT:[$PSS_{(1)}$-*b*-$PPEGMEA_{(x)}$] thin films using a four-point probe. Block-1 and Block-2 showed very similar conductivities of 0.27 and 0.34 S cm^{-1}, respectively. However, Block-4 and Block-6 showed lower conductivities (0.05 and 0.01 S cm^{-1}, respectively), suggesting that the electronic penalty is greater for increasing PPEGMEA lengths (Figure 3a). These values are lower than other studies of PEDOT:PSS blended with PEG/PEO/PPO (e.g., conductivities of 20 S cm^{-1} for 20 wt % of Pluronic 123[59] and 75 S cm^{-1} for 70 wt % PEG 20K).[49] This might suggest that the PPEGMEA segment in our block

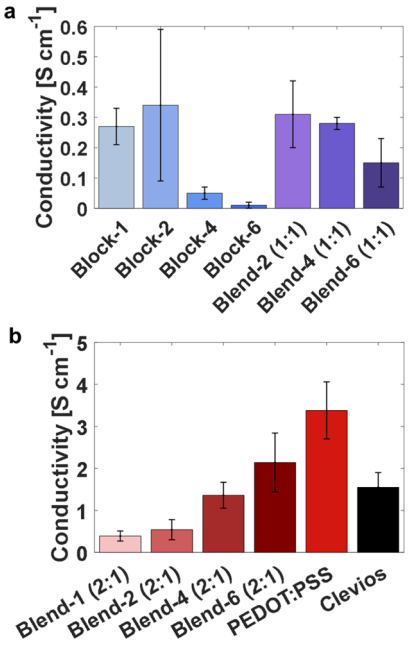

Figure 3. Conductivity of PEDOT:[$PSS_{(1)}$-*b*-$PPEGMEA_{(x)}$] spin-coated thin films measured using a four-point probe. (a) Blocks and blends with a ratio of (1:1). (b) Blends with a ratio of (2:1). The error bars represent the standard deviation from three measured samples.

https://doi.org/10.1021/acsami.1c18495
ACS Appl. Mater. Interfaces 2022, 14, 4823−4835

copolymers does not act as a secondary dopant for the electrical conductivity. However, four-point probe measurements are limited to DC current and do not distinguish between ionic and electronic modes of charge transport. Our block copolymers contain PPEGMEA segments that are composed of repeated polyethers, which have shown good ionic conductivity on their own[60] and as a polar side chains of conjugated polymers.[61−63] Thus, we wanted to evaluate the effect of the PPEGMEA chain length on the impedance and the ionic conductivity. Electrochemical impedance spectroscopy (EIS) was performed on free-standing films of Block-1 to Block-6 sandwiched between two stainless steel electrodes at various frequencies. For all block copolymers, a closed semicircle (common of mixed ionic electronic conductors) was observed in the Nyquist plots (Figure S11b).[64−66] The measured impedance, which contains both the ionic and electronic resistance,[64] decreased as the PPEGMEA chain length increased. Block-1, Block-2, Block-4, and Block-6 had resistance values of 867, 377, 469, and 280 kΩ, respectively. The conductivities of Block-1 to Block-6 were also calculated from EIS (i.e., an AC measurement). Block-1, Block-2, Block-4, and Block-6 showed conductivity values of 5.4×10^{-9}, 1.5×10^{-8}, 2.7×10^{-5}, and 4.3×10^{-5} S cm^{-1}, respectively. These values are similar to other reported PEDOT-based blends.[50] Although four-point measurements showed a consistent decrease in conductivity relative to increasing PPEGMEA chain length, EIS measurements showed an increase in conductivity between Block-1 and Block-6. This trend suggests that the PPEGMEA chains may facilitate ionic charge transfer, and it stands in line with recent studies.[61,62] For example, insulating polymer electrolytes such as poly(ethylene oxide) (PEO) have been shown to improve ionic transport by plasticizing polymers[67] and creating a mobile solvation shell.[68] Similarly, Figure S11c shows that the impedance amplitude decreased as the PPEGMEA chain length increased, with Block-6 possessing the lowest amplitude. Again, this trend may suggest an increase in ionic conductivity with increasing PPEGMEA chain length. Thus, a thorough investigation elucidating the effect of the PPEGMEA segment on the ionic conductivity of PEDOT:PSS should be performed, but it is out of the scope of this article. Therefore, for this paper, we continue to refer to PPEGMEA as an insulating material.

3.3. Blending PEDOT:[PSS$_{(1)}$-*b*-PPEGMEA$_{(x)}$] with PEDOT:PSS. Blend-4 (1:1) and Blend-6 (1:1) had average conductivities of 0.28 and 0.15 S cm^{-1}, respectively, which is a 5- and 15-fold improvement relative to their Block-4 and Block-6 counterparts (Figure 3a). Interestingly, the conductivities of Blend-2 (1:1) and Blend-4 (1:1) were similar to that of Block-1 and Block-2 (Figure 3a). Furthermore, we evaluated blends with higher ratios of PEDOT:PSS relative to the insulating PPEGMEA block (2:1) (Scheme S1). As expected, the conductivity was increased for Blend-1 (2:1), Blend-2 (2:1), Blend-4 (2:1), and Blend-6 (2:1), with values of 0.39, 0.54, 1.36, and 2.14 S cm^{-1}, respectively (Figure 3b). These conductivities are comparable to that of thin films of Clevios (a commercially available formulation of PEDOT:PSS), measured by us to be 1.55 S cm^{-1} (Figure 3b). Notably, the increase in PEDOT:PSS fraction resulted in the blended derivatives having a slightly higher conductivity, despite a significantly greater proportion of insulating segments. The conductivities of Blend-4 (2:1) and Blend-6 (2:1) increased by 27- and 214-fold relative to Block-4 and Block-6 (1.36 and 2.14 vs 0.05 and 0.01 S cm^{-1}, respectively). Notably, the conductivity of Blend-6 (2:1) was similar to that of PEDOT:PSS (3.38 S cm^{-1}), despite a significantly greater proportion of insulating segments. Thus, we show that the conductivity of PEDOT derivatives with long PPEGMEA chains can be increased by blending with PEDOT:PSS.

3.4. Mechanical Properties of the PEDOT:[PSS$_{(1)}$-*b*-PPEGMEA$_{(x)}$] Polymer Library. As expected, we found that increasing the length of the PPEGMEA segment resulted in a lower elastic modulus, lower tensile strength, and higher fracture strain (with the increase in fracture strain likely also attributed in part due to the increase in M_n, Figure 4). These

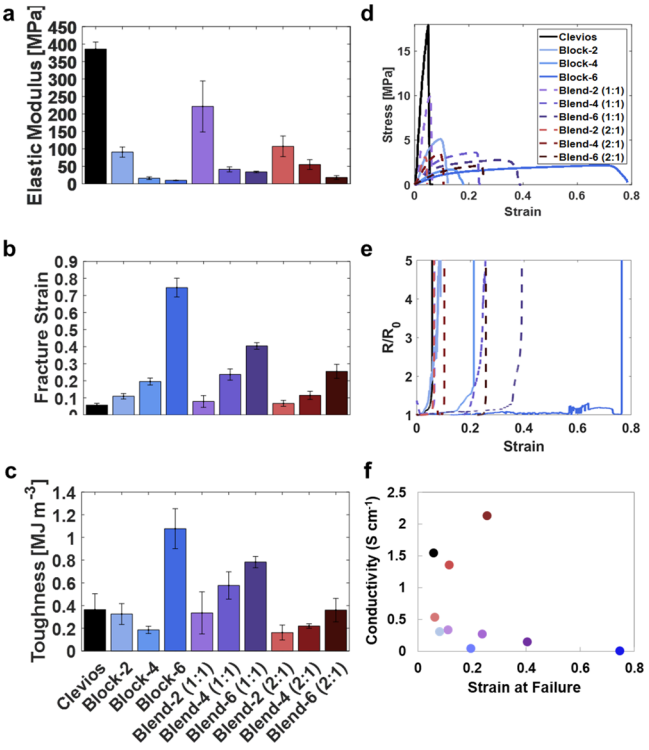

Figure 4. Mechanical properties of the library of PEDOT-based copolymers and copolymer blends. (a) Elastic modulus, (b) fracture strain, and (c) toughness were calculated from three to five tensile tests of each polymer. Error bars shown represent standard deviation. (d) Representative stress−strain curves. (e) Change in resistance (R/R_0) as a function of strain. (f) Conductivity relative to strain at failure. Blend-6 (2:1) (dark brown) showed the highest conductivity, and Block-6 (dark blue) showed the highest fracture strain. Interestingly, Blend-4 (1:1) (purple) showed an increase in both conductivity and fracture strain relative to its Block-4 counterpart.

trends in the tensile behavior are consistent with those observed in polymeric blends by Li et al.[49] Clevios (as a reference) showed brittle behavior, with an average elastic (Young's) modulus of 385 MPa and fracture strain of about 5%, which is similar to that of previously reported PEDOT:PSS dispersions.[51] Block-6 had both the lowest elastic modulus (9 MPa) and highest fracture strain (∼75%) (Figure 4a,b). In comparison, Block-4 and Block-2 had a modulus of 16 and 90 MPa and a fracture strain of 20 and 11%, respectively (Figure 4a,b,d). Notably, increasing the length of the PPEGMEA segment resulted in a large increase in toughness (∼1 MJ m^{-3} for Block-6 compared to ∼0.4 MJ m^{-3} for Clevios) (Figure 4c). Encouragingly, Block-6 showed a lower elastic modulus than that reported for PEDOT:PSS blends, while maintaining a high fracture strain. For example,

https://doi.org/10.1021/acsami.1c18495
ACS Appl. Mater. Interfaces 2022, 14, 4823−4835

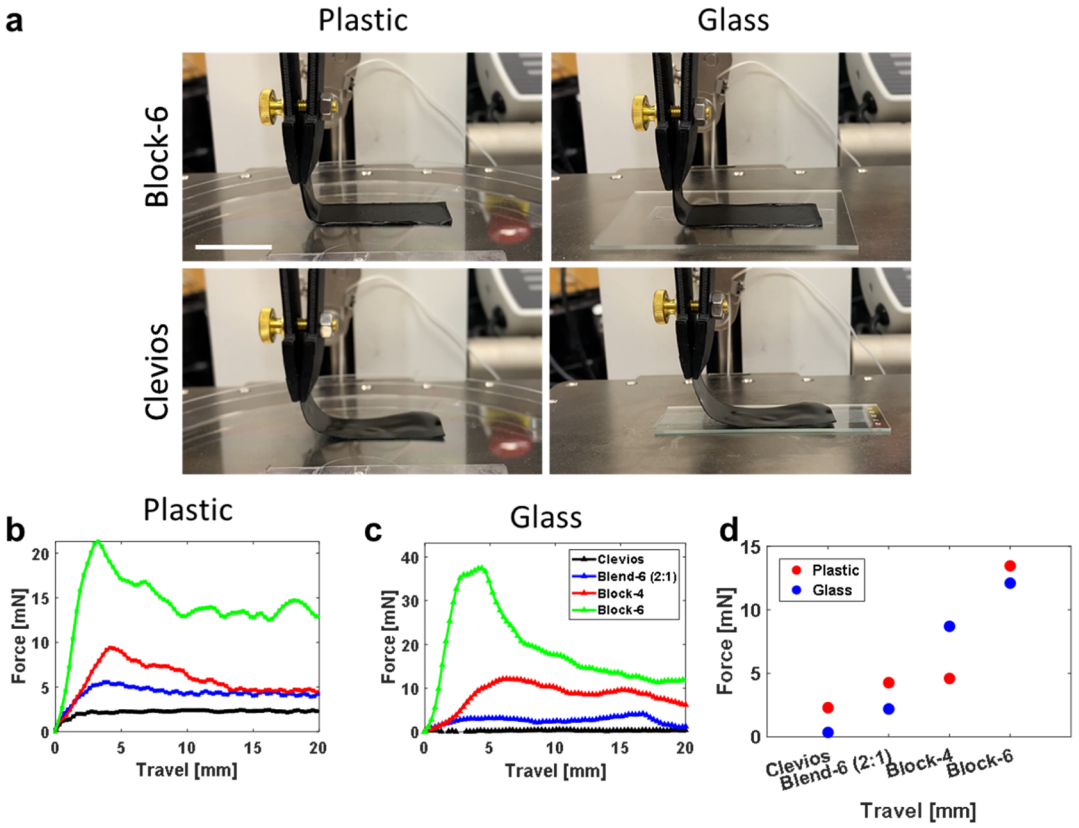

Figure 5. (a) 90° peel tests were performed on free-standing films of Block-6 (upper panels) and Clevios (lower panels) on plastic and glass substrates. The peel tests were conducted with free-standing films of Block-6 (green), Block-4 (red), Blend-6 (2:1) (blue), and Clevios (black) at a speed of 330 mm min^{-1} on a (b) plastic Petri dish and (c) glass microscope slide. (d) Steady-state force required to peel each film off each substrate was extracted and plotted. Block-6, when compared to Blend-6 (2:1), required approximately 3× and 5× as much force to peel off plastic and glass, respectively.

PEDOT:PSS (14 wt %) blended with waterborne polyurethane (WPU) and D-sorbitol had an elastic modulus of ∼40 MPa and fracture strain of ∼70%.[69] Similarly, PEDOT:PSS blended with Pluronic P123, which contains PEO and poly(propylene glycol) (PPO), resulted in a fracture strain of ∼40%.[59] Li et al. showed that PEDOT:PSS blended with 20 kDa PEG or 100 kDa PEO resulted in a fracture strain of 25−27% with a modulus of ∼130 or ∼200 MPa, respectively.[49] Likewise, increasing the molecular weight of the PEO 10-fold to 1000 kDa decreased the modulus to ∼135 MPa and increased the fracture strain to 36%. These values are in contrast to Block-6, which had the lowest elastic modulus (9 MPa) and highest fracture strain (∼75%). Thus, we show that synthetic modification of PEDOT:PSS using a PPEGMEA scaffold can be used to achieve both a low elastic modulus and a high fracture strain, two important mechanical figures of merit for bioelectronic applications.

3.5. Tuning the Electronic and Mechanical Properties of PEDOT:[$PSS_{(1)}$-*b*-$PPEGMEA_{(x)}$] Polymers by blending with PEDOT:PSS. Blending the copolymers with PEDOT:PSS [i.e., Blend-2 (1:1), Blend-4 (1:1), and Blend-6 (1:1)] yielded an embrittling effect, resulting in a higher elastic modulus and decreased fracture strain relative to their nonblended counterparts (i.e., Block-2, Block-4, and Block-6) (Figure 4a,b). For example, the elastic modulus of Blend-6 (1:1) was 32 MPa and the fracture strain was 40% (compared to 9 MPa and 75% for Block-6). Interestingly, Blend-4 (1:1) had not only a higher conductivity (0.28 S cm^{-1}) but also a greater fracture strain (27.3%) and significantly greater toughness (0.57 MJ m^{-3}) than Block-4 (0.05 S cm^{-1}, 20%, 0.18 MJ m^{-3}) (Figure 4b−d). (As expected, Blend-4 (1:1) also had a greater elastic modulus than Block-4.) It is possible that this improvement in both electronic and mechanical properties could be attributed to a more favorable spatial arrangement (e.g., packing structure) of PEDOT:PSS and Block-4. Increasing the ratio of PEDOT:PSS to copolymer (2:1 wt %) generally increased the embrittling effect, particularly for the fracture strains (Figure 4b). However, both Blend-2 (2:1) and Blend-6 (2:1) show a higher conductivity (Figure 3b) and lower modulus (Figure 4a) than their 1:1 blended counterparts. Thus, our results show that blending block copolymers with PEDOT:PSS offers an avenue for tuning (and optimizing) both the mechanical and electronic properties.

3.6. Piezoresistance of PEDOT:[$PSS_{(1)}$-*b*-$PPEGMEA_{(x)}$] Polymers. We measured the change in resistance as a function of strain (i.e., piezoresistance) for each PEDOT derivative shown in Figure 4e. We find that the strain at which an open circuit formed (i.e., strain at failure) correlated strongly with the fracture strain for both copolymers and copolymer blends. That is to say, the change in resistance (R/R_0) for each PEDOT derivative remained approximately constant at 1 as the film elongated without breaking and then increased as a tear propagated through the film. The correlation between conductivity (as measured using a four-point probe) and strain at failure is summarized in Figure 4f.

https://doi.org/10.1021/acsami.1c18495
ACS Appl. Mater. Interfaces 2022, 14, 4823−4835

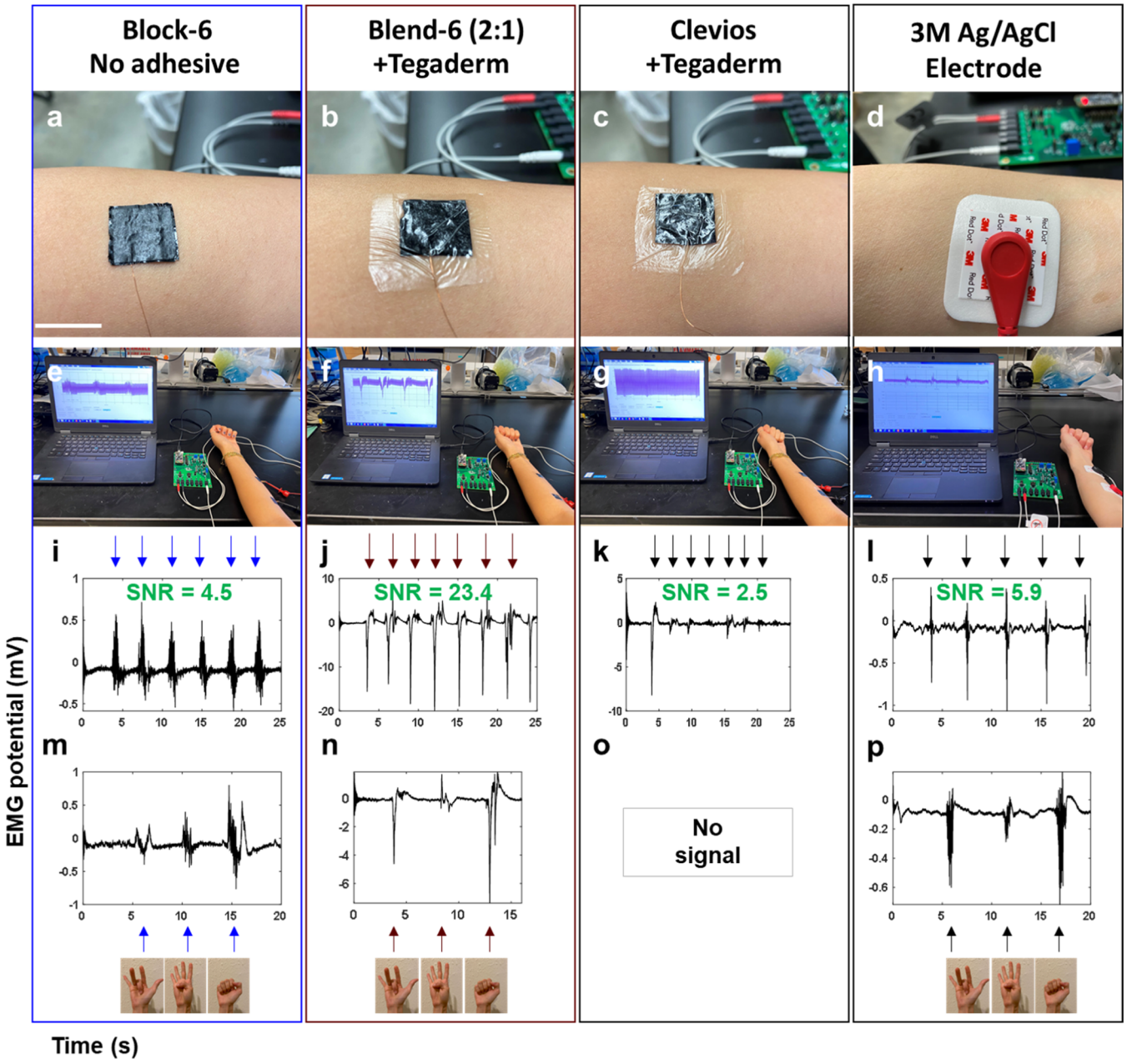

Figure 6. Application of Block-6, Blend-6, and Clevios as single-component sEMG electrodes. Dry EMG electrodes were fabricated using (a) Block-6, (b) Blend-6, and (c) Clevios with (d) a commercially available 3 M Ag/AgCl Monitoring Electrode as a reference. Clevios and Blend-6 needed an adhesive covering (Tegaderm) to tape the electrode to the forearm. The scale bar is 2 cm. (e–h) EMG signals were measured during fist closing motions. The signal was processed using a 60 Hz filter to eliminate powerline noise. (i–l) Arrows pointing down indicate the EMG signal obtained for fist closing motions. SNR values are shown in green. (m,n,p) Arrows pointing up indicate flexion and extension of different fingers. (o) No signal was obtained for the Clevios reference electrode during the flexion and extension of different fingers.

3.7. Application to sEMG Electrodes. Wearable sensors that interface with skin require an elastic modulus similar to that of skin. The modulus of skin on the forearm is reported to be ~1 MPa.[70] Therefore, for sEMG electrodes[69] on the forearm, we chose to compare Block-6 (9 MPa), Blend-6 (1:1) (17 Mpa), and Clevios with a commercial 3 M Ag/AgCl sEMG electrode as a reference. An additional benefit was the improved contact of Block-6 to skin, in comparison with Clevios (Figure S12). This improved conformability for Block-6 is likely due to the reduction in elastic mismatch between the electrode and the skin, resulting in better adhesion (Figure S12 and Movies S2, S3, and S4). Likewise, we find that an increase in PPEGMEA chain length (e.g., Clevios and Block-6) and proportion [e.g., Blend-6 (2:1) and Block-6] results in greater measurable adhesion to both plastic and glass substrates (Figure 5). We note that our peel test measurements of Clevios overestimate the adhesion. The Clevios data indicated similar adhesion to Blend-6 (2:1), despite Movies S5, S6, and S7 indicating negligible adhesion of Clevios to either substrate. We attribute these errors in measurement as artifacts resulting from the deflection of the stiff Clevios film on the substrate (e.g., measurement of a bending force) rather than adhesion to the substrate. Blend-6 (2:1) and Clevios required an adhesive covering (Tegaderm) to tape the electrode to the skin.

https://doi.org/10.1021/acsami.1c18495
ACS Appl. Mater. Interfaces 2022, 14, 4823–4835

However, the Block-6 electrode was sufficiently conformable, likely due to the similar elastic modulus, and functioned as a single-component electrode (i.e., with no adhesive layer applied and no additional additives) on the forearm (Figure 6a–d). After each electrode was secured on the forearm, the EMG signal was monitored for fist opening and closing motions, as well as the flexion and extension of different fingers (Figure 6e–p). Movies S8, S9, S10, and S11 show the EMG signal recorded for the Block-6, Blend-6, Clevios, and the control 3 M Ag/AgCl electrodes, respectively, while clenching a fist. The Block-6 EMG electrode outperformed its Blend-6 (2:1) and Clevios counterparts, demonstrating the most stable baseline when no motion was occurring and a Gaussian peak during muscle activation. In contrast, Blend-6 (2:1) showed a negative baseline change (Figure 6j,n), likely due to contact artifacts and perhaps indicating insufficient contact between the electrode and the skin.[71] In addition, the SNR for Block-6 was slightly lower than that of the commercially available 3 M Ag/AgCl electrode that was used as a control (4.5 vs 5.9, respectively). Blend-6 (2:1) had the highest SNR, probably due to the negative change, which provided the highest RMS (Figures 6i–l, S13). The Clevios electrode had the lowest SNR, likely due to poor contact with the skin (e.g., relatively high elastic modulus). The EMG signal could detect the movement of different fingers for Block-6, Blend-6 (2:1), and the control Ag/AgCl electrode. However, no signal was obtained for the Clevios electrode. Likewise, a significant consideration for wearable sensors that interface with skin is the ability of the device to withstand moisture or sweat (which could promote disintegration of the sensor materials or affect device performance). To assess the physical stability in an aqueous environment, we soaked a spin-coated film of Block-6 in water for 5 days at room temperature and compared it with a Clevios film (as a reference) (Figure S14a–d). The Block-6 films (Figure S14a,c) remained intact in the water bath, whereas the Clevios films dissolved (Figure S14b,d). Thus, we demonstrate that Block-6 outperforms its Clevios counterpart in both function as a (single-component) sEMG electrode and resistance to degradation from water. Zhang et al. recently demonstrated a dry EMG electrode made of PEDOT:PSS (14 wt %) blended with WPU and D-sorbitol for achieving a conductive, adhesive, and stretchable electrode.[69] Our single-component Block-6 sEMG electrode showed a similar fracture strain (~75% in comparison to ~70%) and a lower elastic modulus (9 MPa in comparison to 40 MPa), although the adhesiveness and conductivity were lower. In addition to small molecule and polymeric additives, an alternative approach for increasing the conductivity and modulating the mechanical properties of PEDOT:PSS is the incorporation of biocompatible ILs.[48]

Our device was composed of a bare copper wire directly connected to the PEDOT:PSS film using carbon paint (and carbon tape) for the purpose of demonstrating its application as a sEMG electrode. However, such a structure would not be stable or durable enough for commercial use. Other studies have discussed more sophisticated device structures, as well as elucidated the importance of support layers and stable interconnects.[48]

4. CONCLUSIONS

The purpose of this study was (1) to elucidate the effect of increasing lengths of PPEGMEA covalently bound to PEDOT:PSS on the mechanical and electrical properties and (2) to demonstrate how this synthetic approach can be used to tune the properties of the polymer for bioelectronic applications. We showed that increasing the length of the PPEGMEA segment on the PEDOT:[$PSS_{(1)}$-*b*-$PPEGMEA_{(x)}$] copolymer resulted in a lower elastic modulus, lower tensile strength, higher fracture strain, and greater toughness. In doing so, the conductivity of the polymer film decreased relative to the increasing length of PPEGMEA. However, we found that this conductivity could be restored, and even improved, by blending the PEDOT-based block copolymer with PEDOT:PSS. Although PEDOT:PSS imparts an embrittling effect on the polymer film, some formulations [Blend-4 (1:1) and Blend-6 (2:1)] showed a minimal decrease in mechanical performance. Thus, we show that synthetically altering the PPEGMEA length and blending with PEDOT:PSS offer two avenues for tuning both the mechanical and electronic properties of PEDOT:[$PSS_{(1)}$-*b*-$PPEGMEA_{(x)}$] and its derivatives. Additionally, we demonstrate that Block-6 and Blend-6 (2:1) can be used to fabricate electrodes to monitor EMG signals on the forearm. Block-6 was particularly well suited for this sEMG application due to its low modulus (i.e., comparable to that of forearm skin), good contact to the skin, and good resistance to water (relative to Clevios). One potential limitation of the described PEDOT-based library for bioelectronic applications is the limited conductivity. All PEDOT derivatives presented in this work have relatively low conductivities, with the highest being Blend-6 (2:1) at just over 2 S cm^{-1}. However, this conductivity is still similar to that of Clevios and other commercial PEDOT:PSS formulations, which is generally not used without a secondary dopant. Therefore, for applications where higher conductivities are required and additive leaching is not a potential concern, this PEDOT:[$PSS_{(1)}$-*b*-$PPEGMEA_{(x)}$] library would benefit from the incorporation of common additives used for PEDOT:PSS (as already described by a vast body of literature). For additive-free applications, additional synthetic approaches for increasing the conductivity (e.g., different functional groups, scaffolds, and copolymerization strategies) should be investigated.

■ ASSOCIATED CONTENT

Supporting Information

The Supporting Information is available free of charge at https://pubs.acs.org/doi/10.1021/acsami.1c18495.

UV–vis spectra, ^{1}H NMR spectra, surface morphology by AFM and SEM, Nyquist plot, impedance magnitude versus frequency, free-standing films placed on the human skin, SNR of the dry electrodes, and stability of Block-6 and Clevios in water (PDF)

$PSS_{(1)}$-*b*-$PPEGMEA_{(6)}$ sticky solid (MP4)

Block-6 on plastic (MP4)

Block-6 on glass (MP4)

Block-6 on forearm skin (MP4)

Clevios on plastic (MP4)

Clevios on Glass (MP4)

Clevios on forearm skin (MP4)

EMG signal recorded for the the Block-6 electrodes, while clenching a fist (MP4)

EMG signal recorded for the Blend-6 electrodes, while clenching a fist (MP4)

EMG signal recorded for the Clevios electrodes, while clenching a fist (MP4)

https://doi.org/10.1021/acsami.1c18495
ACS Appl. Mater. Interfaces 2022, 14, 4823–4835

EMG signal recorded for the control 3 M Ag/AgCl electrodes, while clenching a fist (MP4)

AUTHOR INFORMATION

Corresponding Author

Darren J. Lipomi − *Department of NanoEngineering, University of California, San Diego, La Jolla, California 92093-0448, United States;* orcid.org/0000-0002-5808-7765; Email: dlipomi@eng.ucsd.edu

Authors

Rachel Blau − *Department of NanoEngineering, University of California, San Diego, La Jolla, California 92093-0448, United States*

Alexander X. Chen − *Department of NanoEngineering, University of California, San Diego, La Jolla, California 92093-0448, United States;* orcid.org/0000-0003-1919-6755

Beril Polat − *Department of NanoEngineering, University of California, San Diego, La Jolla, California 92093-0448, United States*

Laura L. Becerra − *Department of NanoEngineering, University of California, San Diego, La Jolla, California 92093-0448, United States*

Rory Runser − *Department of NanoEngineering, University of California, San Diego, La Jolla, California 92093-0448, United States*

Beeta Zamanimeymian − *Department of NanoEngineering, University of California, San Diego, La Jolla, California 92093-0448, United States*

Kartik Choudhary − *Department of NanoEngineering, University of California, San Diego, La Jolla, California 92093-0448, United States;* orcid.org/0000-0003-2611-8982

Complete contact information is available at: https://pubs.acs.org/10.1021/acsami.1c18495

Notes

The authors declare no competing financial interest.

ACKNOWLEDGMENTS

This work was supported by the Air Force Office of Scientific Research (AFOSR) grant no. FA9550-19-1-0278. R.B. acknowledges a fellowship from the Zuckerman-CHE STEM Leadership Program and Marie Skłodowska-Curie Actions (MSCA) fellowship. L.L.B. acknowledges support from the National Science Foundation Graduate Research Fellowship (NSF GRFP) under grant no. DGE-2038238. R.R. acknowledges support from the National Science Foundation Graduate Research Fellowship (NSF GRFP) under grant no. DGE-1144086. K.C. acknowledges additional support as a Hellman Scholar and an Intel Scholar provided through the Academic Enrichment Program (AEP) at UCSD through the following awards: The Undergraduate Research Scholarship and Semiconductor Research Corporation Scholarship. We would like to thank Diyi Cheng for his help with ionic conductivity measurements. This work was performed in part at the San Diego Nanotechnology Infrastructure (SDNI), a member of the National Nanotechnology Coordinated Infrastructure, which is supported by the National Science Foundation (grant ECCS-1542148).

REFERENCES

(1) Lin, P.; Yan, F.; Yu, J.; Chan, H. L. W.; Yang, M. The Application of Organic Electrochemical Transistors in Cell-Based Biosensors. *Adv. Mater.* **2010**, *22*, 3655−3660.

(2) Huang, J.; Li, G.; Yang, Y. A Semi-Transparent Plastic Solar Cell Fabricated by a Lamination Process. *Adv. Mater.* **2008**, *20*, 415−419.

(3) Chang, J.-K.; Huang, Y.-Y.; Lin, D.-L.; Tau, J.-I.; Chen, T.-H.; Chen, M.-H. Solution-Processed, Semitransparent Organic Photovoltaics Integrated with Solution-Doped Graphene Electrodes. *Sci. Rep.* **2020**, *10*, 20010.

(4) Zhang, Y.; Peng, Z.; Cai, C.; Liu, Z.; Lin, Y.; Zheng, W.; Yang, J.; Hou, L.; Cao, Y. Colorful Semitransparent Polymer Solar Cells Employing a Bottom Periodic One-Dimensional Photonic Crystal and a Top Conductive PEDOT:PSS Layer. *J. Mater. Chem. A* **2016**, *4*, 11821−11828.

(5) Bag, S.; Durstock, M. F. Efficient semi-transparent planar perovskite solar cells using a 'molecular glue'. *Nano Energy* **2016**, *30*, 542−548.

(6) Liang, J.; Li, L.; Niu, X.; Yu, Z.; Pei, Q. Elastomeric Polymer Light-Emitting Devices and Displays. *Nat. Photonics* **2013**, *7*, 817−824.

(7) Seo, Y. K.; Joo, C. W.; Lee, J.; Han, J. W.; Cho, N. S.; Lim, K. T.; Yu, S.; Kang, M. H.; Yun, C.; Choi, B. H.; Kim, Y. H. Efficient ITO-Free Organic Light-Emitting Diodes Comprising PEDOT:PSS Transparent Electrodes Optimized with 2-Ethoxyethanol and Post Treatment. *Org. Electron.* **2017**, *42*, 348−354.

(8) Xu, S.; Hong, M.; Shi, X.-L.; Wang, Y.; Ge, L.; Bai, Y.; Wang, L.; Dargusch, M.; Zou, J.; Chen, Z.-G. High-Performance PEDOT:PSS Flexible Thermoelectric Materials and Their Devices by Triple Post-Treatments. *Chem. Mater.* **2019**, *31*, 5238−5244.

(9) Jiang, Q.; Lan, X.; Liu, C.; Shi, H.; Zhu, Z.; Zhao, F.; Xu, J.; Jiang, F. High-Performance Hybrid Organic Thermoelectric SWNTs/PEDOT:PSS Thin-Films for Energy Harvesting. *Mater. Chem. Front.* **2018**, *2*, 679−685.

(10) Rivnay, J.; Inal, S.; Collins, B. A.; Sessolo, M.; Stavrinidou, E.; Strakosas, X.; Tassone, C.; Delongchamp, D. M.; Malliaras, G. G. Structural Control of Mixed Ionic and Electronic Transport in Conducting Polymers. *Nat. Commun.* **2016**, *7*, 11287.

(11) Savva, A.; Wustoni, S.; Inal, S. Ionic-to-Electronic Coupling Efficiency in PEDOT:PSS Films Operated in Aqueous Electrolytes. *J. Mater. Chem. C* **2018**, *6*, 12023−12030.

(12) Roshanbinfar, K.; Vogt, L.; Greber, B.; Diecke, S.; Boccaccini, A. R.; Scheibel, T.; Engel, F. B.; Diecke, S.; Boccaccini, A. R.; Scheibel, T.; Engel, F. B.; Greber, B.; Diecke, S.; Scheibel, T. Electroconductive Biohybrid Hydrogel for Enhanced Maturation and Beating Properties of Engineered Cardiac Tissues. *Adv. Funct. Mater.* **2018**, *28*, 1803951.

(13) Nilsson, D.; Robinson, N.; Berggren, M.; Forchheimer, R.; Baldo, M. A.; You, Y.; Shoustikov, A.; Sib-ley, S.; Thompson, M. E.; Forrest, S. R.; Ma, Y. G.; Zhang, H. Y.; Shen, J. C.; Che, C. M.; Met, S.; Jiang, X. Z.; Y Jen, A. K.; Carlson, B.; Dalton, L. R.; Lamansky, S.; Djurovich, P.; Murphy, D.; Abdel-Razzaq, F.; Lee, H.; Adachi, C.; Burrows, P. E.; Xie, H. Z.; Liu, M. W.; Wang, O. Y.; Zhang, X. H.; Lee, C. S.; Hung, L. S.; Lee, S. T.; Teng, P. F.; Kwong, H. L.; Zheng, H.; Anthopoulos, T. D.; J Markham, J. P.; Namdas, E. B.; W Samuel, I. D.; S Paulose, M. J.; Rayabarapu, D. K.; Duan, J.; Cheng, C.; Huang, W.; Shanmugasundaram, M.; Chang, H.; David Nilsson, B.; Robinson, N.; Berggren, M.; Forchheimer, R.; Berggren, M.; Nilsson, D.; Robinson, N.; Forchheimer, R. Electrochemical Logic Circuits. *Adv. Mater.* **2005**, *17*, 353−358.

(14) Inal, S.; Malliaras, G. G.; Rivnay, J. Benchmarking Organic Mixed Conductors for Transistors. *Nat. Commun.* **20172017**, *8*, 1−7.

(15) Gkoupidenis, P.; Schaefer, N.; Garlan, B.; Malliaras, G. G. Neuromorphic Functions in PEDOT:PSS Organic Electrochemical Transistors. *Adv. Mater.* **2015**, *27*, 7176.

(16) Gueye, M. N.; Carella, A.; Faure-Vincent, J.; Demadrille, R.; Simonato, J.-P. Progress in Understanding Structure and Transport Properties of PEDOT-Based Materials: A Critical Review. *Prog. Mater. Sci.* **2020**, *108*, 100616.

(17) Diah, A. W. M.; Quirino, J. P.; Belcher, W.; Holdsworth, C. I. An Assessment of the Effect of Synthetic and Doping Conditions on the Processability and Conductivity of Poly(3,4-Ethylenedioxythiophene)/Poly(Styrene Sulfonic Acid). *Macromol. Chem. Phys.* **2016**, *217*, 1907−1916.
(18) Shi, H.; Liu, C. C.; Jiang, Q. L.; Xu, J. K. Effective Approaches to Improve the Electrical Conductivity of PEDOT:PSS: A Review. *Adv. Electron. Mater.* **2015**, *1*, 1500017.
(19) Malti, A.; Edberg, J.; Granberg, H.; Khan, Z. U.; Andreasen, J. W.; Liu, X.; Zhao, D.; Zhang, H.; Yao, Y.; Brill, J. W.; Engquist, I.; Fahlman, M.; Wågberg, L.; Crispin, X.; Berggren, M.; Edberg, J.; Khan, Z. U.; Zhao, D.; Engquist, I.; Crispin, X.; Berggren, M.; Granberg, H.; Andreasen, J. W.; Liu, X.; Fahlman, M.; Zhang, H.; Yao, Y.; Brill, J. W.; Wågberg, L. An Organic Mixed Ion−Electron Conductor for Power Electronics. *Adv. Sci.* **2016**, *3*, 1500305.
(20) Nardes, A. M.; Kemerink, M.; de Kok, M. M.; Vinken, E.; Maturova, K.; Janssen, R. A. J. J. Conductivity, Work Function, and Environmental Stability of PEDOT:PSS Thin Films Treated with Sorbitol. *Org. Electron.* **2008**, *9*, 727−734.
(21) Kim, N.; Kee, S.; Lee, S. H.; Lee, B. H.; Kahng, Y. H.; Jo, Y.-R.; Kim, B.-J.; Lee, K. Highly Conductive PEDOT:PSS Nanofibrils Induced by Solution-Processed Crystallization. *Adv. Mater.* **2014**, *26*, 2268−2272.
(22) Xia, Y.; Sun, K.; Ouyang, J.; Xia, Y.; Sun, K.; Ouyang, J. Solution-Processed Metallic Conducting Polymer Films as Transparent Electrode of Optoelectronic Devices. *Adv. Mater.* **2012**, *24*, 2436−2440.
(23) Wang, Y.; Zhu, C.; Pfattner, R.; Yan, H.; Jin, L.; Chen, S.; Molina-Lopez, F.; Lissel, F.; Liu, J.; Rabiah, N. I.; Chen, Z.; Chung, J. W.; Linder, C.; Toney, M. F.; Murmann, B.; Bao, Z. A Highly Stretchable, Transparent, and Conductive Polymer. *Sci. Adv.* **2017**, *3*, No. e1602076.
(24) Huang, J.; Miller, P. F.; de Mello, J. C.; de Mello, A. J.; Bradley, D. D. C. Influence of Thermal Treatment on the Conductivity and Morphology of PEDOT/PSS Films. *Synth. Met.* **2003**, *139*, 569−572.
(25) Su, Z.; Wang, L.; Li, Y.; Zhao, H.; Chu, B.; Li, W. Ultraviolet-Ozone-Treated PEDOT:PSS as Anode Buffer Layer for Organic Solar Cells. *Nanoscale Res. Lett.* **2012**, *7*, 1−6.
(26) Teo, M. Y.; Kim, N.; Kee, S.; Kim, B. S.; Kim, G.; Hong, S.; Jung, S.; Lee, K. Highly Stretchable and Highly Conductive PEDOT:PSS/Ionic Liquid Composite Transparent Electrodes for Solution-Processed Stretchable Electronics. *ACS Appl. Mater. Interfaces* **2017**, *9*, 819−826.
(27) Meng, W.; Ge, R.; Li, Z.; Tong, J.; Liu, T.; Zhao, Q.; Xiong, S.; Jiang, F.; Mao, L.; Zhou, Y. Conductivity Enhancement of PEDOT:PSS Films via Phosphoric Acid Treatment for Flexible All-Plastic Solar Cells. *ACS Appl. Mater. Interfaces* **2015**, *7*, 14089−14094.
(28) Bießmann, L.; Saxena, N.; Hohn, N.; Hossain, M. A.; Veinot, J. G. C.; Müller-Buschbaum, P. Highly Conducting, Transparent PEDOT:PSS Polymer Electrodes from Post-Treatment with Weak and Strong Acids. *Adv. Electron. Mater.* **2019**, *5*, 1800654.
(29) Zhang, L.; Yang, K.; Chen, R.; Zhou, Y.; Chen, S.; Zheng, Y.; Li, M.; Xu, C.; Tang, X.; Zang, Z.; Sun, K. The Role of Mineral Acid Doping of PEDOT:PSS and Its Application in Organic Photovoltaics. *Adv. Electron. Mater.* **2020**, *6*, 1900648.
(30) Timpanaro, S.; Kemerink, M.; Touwslager, F. J.; De Kok, M. M.; Schrader, S. Morphology and Conductivity of PEDOT/PSS Films Studied by Scanning-Tunneling Microscopy. *Chem. Phys. Lett.* **2004**, *394*, 339−343.
(31) Crispin, X.; Jakobsson, F. L. E.; Crispin, A.; Grim, P. C. M.; Andersson, P.; Volodin, A.; van Haesendonck, C.; Van der Auweraer, M.; Salaneck, W. R.; Berggren, M. The Origin of the High Conductivity of Poly(3,4-ethylenedioxythiophene)−Poly-(styrenesulfonate) (PEDOT−PSS) Plastic Electrodes. *Chem. Mater.* **2006**, *18*, 4354−4360.
(32) Kim, J. Y.; Jung, J. H.; Lee, D. E.; Joo, J. Enhancement of Electrical Conductivity of Poly(3,4-Ethylenedioxythiophene)/Poly(4-Styrenesulfonate) by a Change of Solvents. *Synth. Met.* **2002**, *126*, 311−316.
(33) Ouyang, J.; Xu, Q.; Chu, C.-W.; Yang, Y.; Li, G.; Shinar, J. On the Mechanism of Conductivity Enhancement in Poly(3,4-Ethylenedioxythiophene):Poly(Styrene Sulfonate) Film through Solvent Treatment. *Polymer* **2004**, *45*, 8443−8450.
(34) Alemu Mengistie, D.; Wang, P.-C.; Chu, C.-W. Effect of Molecular Weight of Additives on the Conductivity of PEDOT:PSS and Efficiency for ITO-Free Organic Solar Cells. *J. Mater. Chem. A* **2013**, *1*, 9907−9915.
(35) Nevrela, J.; Micjan, M.; Novota, M.; Kovacova, S.; Pavuk, M.; Juhasz, P.; Kovac, J.; Jakabovic, J.; Weis, M. Secondary Doping in Poly(3,4-Ethylenedioxythiophene):Poly(4-Styrenesulfonate) Thin Films. *J. Polym. Sci., Part B: Polym. Phys.* **2015**, *53*, 1139−1146.
(36) Palumbiny, C. M.; Liu, F.; Russell, T. P.; Hexemer, A.; Wang, C.; Müller-Buschbaum, P. The Crystallization of PEDOT:PSS Polymeric Electrodes Probed In Situ during Printing. *Adv. Mater.* **2015**, *27*, 3391−3397.
(37) Kalra, A.; Lowe, A. Mechanical Behaviour of Skin: A Review. *J. Mater. Sci. Eng.* **2016**, *5*, 1000254.
(38) Feron, K.; Lim, R.; Sherwood, C.; Keynes, A.; Brichta, A.; Dastoor, P. Organic Bioelectronics: Materials and Biocompatibility. *Int. J. Mol. Sci.* **2018**, *19*, 2382.
(39) Someya, T.; Bao, Z.; Malliaras, G. G. The Rise of Plastic Bioelectronics. *Nature* **2016**, *540*, 379−385.
(40) Root, S. E.; Savagatrup, S.; Printz, A. D.; Rodriquez, D.; Lipomi, D. J. Mechanical Properties of Organic Semiconductors for Stretchable, Highly Flexible, and Mechanically Robust Electronics. *Chem. Rev.* **2017**, *117*, 6467−6499.
(41) Kim, D.-H.; Lu, N.; Ma, R.; Kim, Y.-S.; Kim, R.-H.; Wang, S.; Wu, J.; Won, S. M.; Tao, H.; Islam, A.; Yu, K. J.; Kim, T.-i.; Chowdhury, R.; Ying, M.; Xu, L.; Li, M.; Chung, H.-J.; Keum, H.; McCormick, M.; Liu, P.; Zhang, Y.-W.; Omenetto, F. G.; Huang, Y.; Coleman, T.; Rogers, J. A. Epidermal Electronics. *Science 80-* **2011**, *333*, 838.
(42) Mengüç, Y.; Park, Y.-L.; Pei, H.; Vogt, D.; Aubin, P. M.; Winchell, E.; Fluke, L.; Stirling, L.; Wood, R. J.; Walsh, C. J. Wearable Soft Sensing Suit for Human Gait Measurement. *Int. J. Robot Res.* **2014**, *33*, 1748−1764.
(43) Lipomi, D. J. Stretchable Figures of Merit in Deformable Electronics. *Adv. Mater.* **2016**, *28*, 4180−4183.
(44) Li, Y.; Tanigawa, R.; Okuzaki, H. Soft and Flexible PEDOT/PSS Films for Applications to Soft Actuators. *Smart Mater. Struct.* **2014**, *23*, 074010.
(45) Savagatrup, S.; Chan, E.; Renteria-Garcia, S. M.; Printz, A. D.; Zaretski, A. V.; O'Connor, T. F.; Rodriquez, D.; Valle, E.; Lipomi, D. J. Plasticization of PEDOT:PSS by Common Additives for Mechanically Robust Organic Solar Cells and Wearable Sensors. *Adv. Funct. Mater.* **2015**, *25*, 427−436.
(46) He, H.; Zhang, L.; Guan, X.; Cheng, H.; Liu, X.; Yu, S.; Wei, J.; Ouyang, J. Biocompatible Conductive Polymers with High Conductivity and High Stretchability. *ACS Appl. Mater. Interfaces* **2019**, *11*, 26185−26193.
(47) Jönsson, S. K. M.; Birgerson, J.; Crispin, X.; Greczynski, G.; Osikowicz, W.; Denier van der Gon, A. .; Salaneck, W. .; Fahlman, M. The Effects of Solvents on the Morphology and Sheet Resistance in Poly(3,4-Ethylenedioxythiophene)−Polystyrenesulfonic Acid (PEDOT−PSS) Films. *Synth. Met.* **2003**, *139*, 1−10.
(48) Velasco-Bosom, S.; Karam, N.; Carnicer-Lombarte, A.; Gurke, J.; Casado, N.; Tomé, L. C.; Mecerreyes, D.; Malliaras, G. G. Conducting Polymer-Ionic Liquid Electrode Arrays for High-Density Surface Electromyography. *Adv. Healthcare Mater.* **2021**, *10*, 2100374.
(49) Li, P.; Sun, K.; Ouyang, J. Stretchable and Conductive Polymer Films Prepared by Solution Blending. *ACS Appl. Mater. Interfaces* **2015**, *7*, 18415−18423.
(50) Chen, C.-h.; Kine, A.; Nelson, R. D.; LaRue, J. C. Impedance Spectroscopy Study of Conducting Polymer Blends of PEDOT:PSS and PVA. *Synth. Met.* **2015**, *206*, 106−114.
(51) Kayser, L. V.; Lipomi, D. J. Stretchable Conductive Polymers and Composites Based on PEDOT and PEDOT:PSS. *Adv. Mater.* **2019**, *31*, 1806133.

https://doi.org/10.1021/acsami.1c18495
ACS Appl. Mater. Interfaces 2022, 14, 4823−4835

(52) Yang, Y.; Deng, H.; Fu, Q. Recent Progress on PEDOT:PSS Based Polymer Blends and Composites for Flexible Electronics and Thermoelectric Devices. *Mater. Chem. Front.* **2020**, *4*, 3130−3152.
(53) Kayser, L. V.; Russell, M. D.; Rodriquez, D.; Abuhamdieh, S. N.; Dhong, C.; Khan, S.; Stein, A. N.; Ramírez, J.; Lipomi, D. J. RAFT Polymerization of an Intrinsically Stretchable Water-Soluble Block Copolymer Scaffold for PEDOT. *Chem. Mater.* **2018**, *30*, 4459−4468.
(54) Keef, C. V.; Kayser, L. V.; Tronboll, S.; Carpenter, C. W.; Root, N. B.; Finn, M.; O'Connor, T. F.; Abuhamdieh, S. N.; Davies, D. M.; Runser, R.; Meng, Y. S.; Ramachandran, V. S.; Lipomi, D. J. Virtual Texture Generated Using Elastomeric Conductive Block Copolymer in a Wireless Multimodal Haptic Glove. *Adv. Intell. Syst.* **2020**, *2*, 2000018.
(55) Sen, A. K.; Roy, S.; Juvekar, V. A. Effect of Structure on Solution and Interfacial Properties of Sodium Polystyrene Sulfonate (NaPSS). *Polym. Int.* **2007**, *56*, 167−174.
(56) Perrier, S. 50th Anniversary Perspective: RAFT Polymerization-A User Guide. *Macromolecules* **2017**, *50*, 7433−7447.
(57) Miccoli, I.; Edler, F.; Pfnür, H.; Tegenkamp, C. The 100th Anniversary of the Four-Point Probe Technique: The Role of Probe Geometries in Isotropic and Anisotropic Systems. *J. Phys.: Condens. Matter* **2015**, *27*, 223201.
(58) Kher, R. Signal Processing Techniques for Removing Noise from ECG Signals. *J. Biomed. Eng.* **2019**, *3*, NA.
(59) Lee, J. H.; Jeong, Y. R.; Lee, G.; Jin, S. W.; Lee, Y. H.; Hong, S. Y.; Park, H.; Kim, J. W.; Lee, S.-S.; Ha, J. S. Highly Conductive, Stretchable, and Transparent PEDOT:PSS Electrodes Fabricated with Triblock Copolymer Additives and Acid Treatment. *ACS Appl. Mater. Interfaces* **2018**, *10*, 28027−28035.
(60) Olmedo-Martínez, J.; Meabe, L.; Basterretxea, A.; Mecerreyes, D.; Müller, A. Effect of Chemical Structure and Salt Concentration on the Crystallization and Ionic Conductivity of Aliphatic Polyethers. *Polymers* **2019**, *11*, 452.
(61) Giovannitti, A.; Sbircea, D.-T.; Inal, S.; Nielsen, C. B.; Bandiello, E.; Hanifi, D. A.; Sessolo, M.; Malliaras, G. G.; McCulloch, I.; Rivnay, J. Controlling the Mode of Operation of Organic Transistors through Side-Chain Engineering. *Proc. Natl. Acad. Sci. U.S.A.* **2016**, *113*, 12017−12022.
(62) Nielsen, C. B.; Giovannitti, A.; Sbircea, D.-T.; Bandiello, E.; Niazi, M. R.; Hanifi, D. A.; Sessolo, M.; Amassian, A.; Malliaras, G. G.; Rivnay, J.; McCulloch, I. Molecular Design of Semiconducting Polymers for High-Performance Organic Electrochemical Transistors. *J. Am. Chem. Soc.* **2016**, *138*, 10252−10259.
(63) Moia, D.; Giovannitti, A.; Szumska, A. A.; Maria, I. P.; Rezasoltani, E.; Sachs, M.; Schnurr, M.; Barnes, P. R. F.; McCulloch, I.; Nelson, J. Design and Evaluation of Conjugated Polymers with Polar Side Chains as Electrode Materials for Electrochemical Energy Storage in Aqueous Electrolytes. *Energy Environ. Sci.* **2019**, *12*, 1349−1357.
(64) Wieland, M.; Dingler, C.; Merkle, R.; Maier, J.; Ludwigs, S. Humidity-Controlled Water Uptake and Conductivities in Ion and Electron Mixed Conducting Polythiophene Films. *ACS Appl. Mater. Interfaces* **2020**, *12*, 6742−6751.
(65) Nuramdhani, I.; Gokceoren, A.; Odhiambo, S.; De Mey, G.; Hertleer, C.; Van Langenhove, L. Electrochemical Impedance Analysis of a PEDOT:PSS-Based Textile Energy Storage Device. *Materials* **2018**, *11*, 48.
(66) Huggins, R. A. Simple Method to Determine Electronic Conductivity in Mixed A Review and Ionic Components of the Conductors. *Ionics* **2002**, *8*, 300−313.
(67) Xue, Z.; He, D.; Xie, X. Poly(Ethylene Oxide)-Based Electrolytes for Lithium-Ion Batteries. *J. Mater. Chem. A* **2015**, *3*, 19218−19253.
(68) Paulsen, B. D.; Fabiano, S.; Rivnay, J. Mixed Ionic-Electronic Transport in Polymers. *Annu. Rev. Mater. Res.* **2021**, *51*, 73−99.
(69) Zhang, L.; Kumar, K. S.; He, H.; Cai, C. J.; He, X.; Gao, H.; Yue, S.; Li, C.; Seet, R. C.-S.; Ren, H.; Ouyang, J. Fully Organic Compliant Dry Electrodes Self-Adhesive to Skin for Long-Term Motion-Robust Epidermal Biopotential Monitoring. *Nat. Commun.* **2020**, *11*, 1−13.
(70) Escoffier, C.; de Rigal, J.; Rochefort, A.; Vasselet, R.; Lévêque, J.-L.; Agache, P. G. Age-Related Mechanical Properties of Human Skin: An in Vivo Study. *J. Invest. Dermatol.* **1989**, *93*, 353−357.
(71) Zhang, X.; Huang, H. A Real-Time, Practical Sensor Fault-Tolerant Module for Robust EMG Pattern Recognition. *J. NeuroEng. Rehabil.* **2015**, *12*, 1−16.

Recommended by ACS

Developing Stretchable and Photo-Responsive Conductive Films by Incorporation of Spiropyran into Poly(ionic liquid)s
Chia-Wei Chang, Jiun-Tai Chen, *et al.*
MAY 25, 2023
ACS APPLIED POLYMER MATERIALS
READ

Imparting High Conductivity to 3D Printed PEDOT:PSS
Ian M. Hill, Yue Wang, *et al.*
MAY 22, 2023
ACS APPLIED POLYMER MATERIALS
READ

Electrochemical and Solvent-Driven Swelling in a Conducting Polymer Film
Loren G. Kaake, Sabine Ludwigs, *et al.*
MAY 24, 2023
CHEMISTRY OF MATERIALS
READ

What Can We Learn about PEDOT:PSS Morphology from Molecular Dynamics Simulations of Ionic Diffusion?
Tahereh Sedghamiz, Igor Zozoulenko, *et al.*
JULY 05, 2023
CHEMISTRY OF MATERIALS
READ

Get More Suggestions >

https://doi.org/10.1021/acsami.1c18495
ACS Appl. Mater. Interfaces 2022, 14, 4823−4835